Matrix metalloproteinase 9 modulates collagen matrices and wound repair

Danny C. LeBert[1], Jayne M. Squirrell[2], Julie Rindy[3], Elizabeth Broadbridge[3], Yuming Lui[2], Anna Zakrzewska[4], Kevin W. Eliceiri[2], Annemarie H. Meijer[4] and Anna Huttenlocher[3,5,*]

ABSTRACT

Acute and chronic injuries are characterized by leukocyte infiltration into tissues. Although matrix metalloproteinase 9 (Mmp9) has been implicated in both conditions, its role in wound repair remains unclear. We previously reported a zebrafish chronic inflammation mutant caused by an insertion in the hepatocyte growth factor activator inhibitor gene 1 (*hai1*; also known as *spint1*) that is characterized by epithelial extrusions and neutrophil infiltration into the fin. Here, we performed a microarray analysis and found increased inflammatory gene expression in the mutant larvae, including a marked increase in *mmp9* expression. Depletion of *mmp9* partially rescued the chronic inflammation and epithelial phenotypes, in addition to restoring collagen fiber organization, as detected by second-harmonic generation imaging. Additionally, we found that acute wounding induces epithelial cell *mmp9* expression and is associated with a thickening of collagen fibers. Interestingly, depletion of *mmp9* impaired this collagen fiber reorganization. Moreover, *mmp9* depletion impaired tissue regeneration after tail transection, implicating Mmp9 in acute wound repair. Thus, Mmp9 regulates both acute and chronic tissue damage and plays an essential role in collagen reorganization during wound repair.

KEY WORDS: Mmp9, Inflammation, Repair, SHG imaging, Zebrafish

INTRODUCTION

Acute tissue damage is characterized by the infiltration of leukocytes that clear pathogens and cellular debris, followed by wound repair (Lieschke et al., 2001; Nathan, 2006; van Furth et al., 1985). Interestingly, many of the molecular signals induced by acute tissue damage, including chemokines and proteases, are also present in chronic tissue damage, suggesting that tight regulation of wound signaling is crucial for wound resolution (Feghali and Wright, 1997). However, the relationship between the molecular signals induced during acute and chronic tissue damage remains unclear.

A key step during normal repair includes the deposition of collagen to form a transient extracellular matrix (ECM) that is subsequently degraded during the remodeling phase (McCarty and Percival, 2013). Specific proteases, such as the matrix metalloproteinases (MMPs), mediate collagen remodeling during tissue repair and are upregulated during both acute and chronic

wounding (Castaneda et al., 2005; Fini et al., 1996; Mohan et al., 2002; Vandooren et al., 2013). In particular, Mmp9 is associated with many inflammatory processes, including cardiovascular disease and stroke, as well as epithelial injuries to the eye, skin, gut and lung in various organisms ranging from humans to zebrafish (Bai et al., 2005; Betsuyaku et al., 2000; Castaneda et al., 2005; Fini et al., 1996; Mohan et al., 2002; Wyatt et al., 2009). Mmp9 plays an important role in proper keratinocyte migration *in vitro* (Hattori et al., 2009) and *Mmp9* knockout mice display impaired wound closure (McCawley et al., 1998). In both axolotl and zebrafish, *mmp9* expression increases along the wounded edge of the epithelium during early regeneration (Yang et al., 1999; Yoshinari et al., 2009), suggesting a role for Mmp9 during wound healing.

We previously reported zebrafish mutants with chronic epithelial damage and inflammation caused by insertion in the hepatocyte growth factor activator inhibitor gene 1 (*hai1*; also known as *spint1*) (Mathias et al., 2007) or the ENTH domain protein *clint1* (Dodd et al., 2009). Both mutants are reminiscent of the human condition psoriasis, and exhibit epithelial extrusions, hyperproliferation and chronic neutrophil infiltration into the fin (Mathias et al., 2007). In the current study, we aimed to identify factors that contribute to this chronic tissue damage phenotype. We performed a microarray analysis and found a significant increase in *mmp9* expression. Depletion of Mmp9 partially rescued the chronic epithelial damage phenotype.

To investigate the role of Mmp9 during wound repair we used second-harmonic generation (SHG) imaging (Campagnola et al., 2002) to non-invasively assess collagen fiber organization in *hai1* morphants. We found that depletion of *mmp9* partially rescued the disordered collagen fibers observed in the mutant larvae, suggesting that Mmp9 modulates the organization of collagen matrices. By contrast, depletion of *mmp9* impaired regeneration after acute wounding, suggesting that Mmp9 is required for acute wound healing and regeneration in larval zebrafish. Furthermore, with SHG imaging, we determined that *mmp9* expression regulates the transition in collagen fiber thickness that occurs during acute wound healing. Thus, *mmp9* expression differentially regulates acute and chronic tissue damage and repair, and modulates collagen reorganization during wound repair.

RESULTS

hai1 and *clint1* mutants have increased *mmp9* expression

Previous studies from our laboratory identified mutants characterized by chronic epithelial cell damage and persistent neutrophilic infiltration in the epidermis (Dodd et al., 2009; Mathias et al., 2007). To identify mechanisms that contribute to the chronic wound phenotype, we performed microarray analysis of the *hai1 (hi2217)* and *clint1 (hi1520)* mutants. Analysis of RNA from 3 days post-fertilization (dpf) *hi1520* and *hi2217* mutant larvae revealed

[1]Cellular and Molecular Pathology Graduate Program, University of Wisconsin-Madison, Madison, WI 53706, USA. [2]Laboratory for Optical and Computational Instrumentation, University of Wisconsin-Madison, Madison, WI 53706, USA. [3]Department of Medical Microbiology and Immunology, University of Wisconsin-Madison, Madison, WI 53706, USA. [4]Institute of Biology, Leiden University, Einsteinweg 55, 2333 CC, Leiden, The Netherlands. [5]Department of Pediatrics, University of Wisconsin-Madison, Madison, WI 53706, USA.

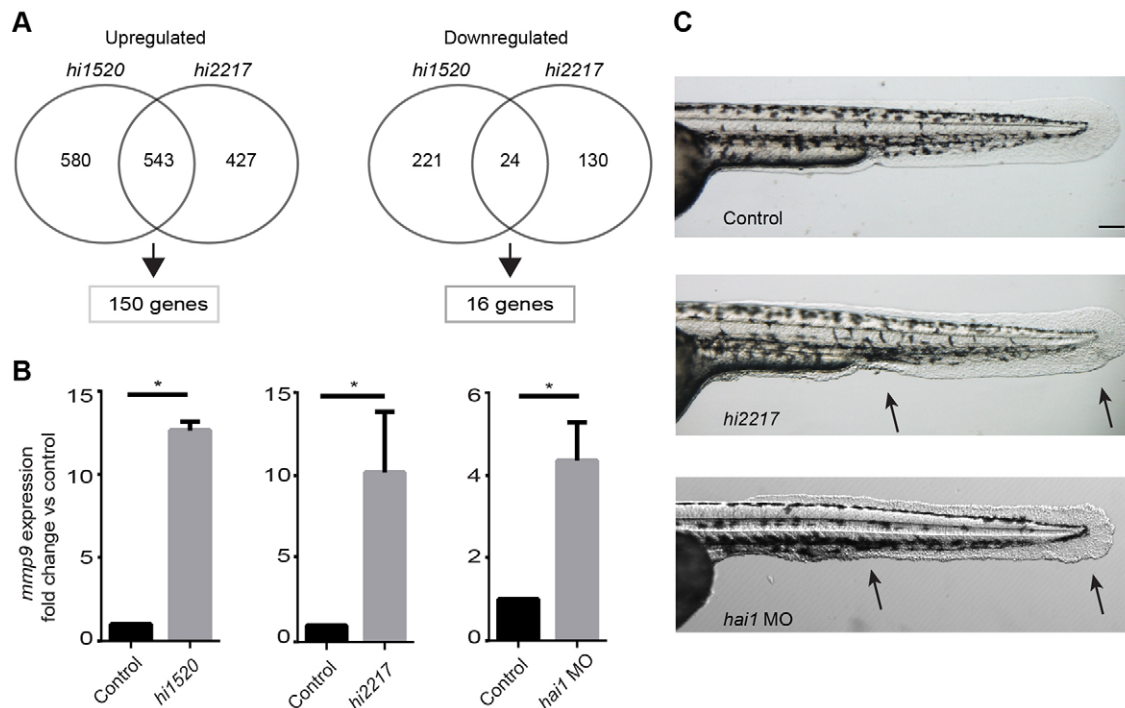*Author for correspondence (huttenlocher@wisc.edu)

Fig. 1. Gene expression profiling reveals elevated inflammatory gene expression, including *mmp9,* in chronic inflammation mutants. (A) Microarray analysis of inflammation mutants, *hi1520* and *hi2217*, revealed overlapping upregulation of 150 genes and downregulation of 16 genes compared with WT siblings. (B) Upregulation of *mmp9* was confirmed by qRT-PCR in the *hi2217* and *hi1520* mutants and the *hai1* morphants. (C) The mutants are characterized by epithelial extrusions and abnormal epithelium development (arrows). Data pooled from experiments performed in triplicate. *$P<0.05$. Scale bar: 200 µm.

166 differentially expressed genes relative to sibling wild-type (WT) larvae (Fig. 1A; supplementary material Fig. S1A,B). We focused on genes involved in pro-inflammatory signaling that modulate ECM remodeling. The most highly overexpressed gene, *mmp9*, was selected for further analysis. Using quantitative real-time PCR (qRT-PCR) we found a significant overexpression of *mmp9* in both the *hi2217* (Fig. 1B) and *hi1520* mutants (Fig. 1B), which was confirmed by *in situ* hybridization of *hi2217* mutant embryos and their WT siblings (supplementary material Fig. S1C). The heterozygous mutant crosses for the *hi2217* fish yield ~25% of larvae with epithelial defects. To achieve a higher percentage of larvae with the *hai1* mutant phenotype, we used a previously established MO to deplete *hai1*, which recapitulates the mutant phenotype (Carney et al., 2007; Mathias et al., 2007). The *hai1* morphants also showed increased *mmp9* expression (Fig. 1B), as determined by qRT-PCR.

Mmp9 depletion partially rescues the *hai1* mutant phenotype

Activation of Mmp9 plays an important role during ECM remodeling (Collier et al., 1988; Fosang et al., 1992; Senior et al., 1991) and restoration of epithelial morphology after tissue damage (Yoshinari et al., 2009). Moreover, inhibition of Mmp9 activity reduces the inflammatory response (Volkman et al., 2010). To determine whether Mmp9 contributes to the abnormal epithelial morphology (Fig. 1C) and neutrophil infiltration (Fig. 2A) observed in the *hai1* morphants, we depleted Mmp9 (Fig. 2B) in the *hai1* mutants using a previously published *mmp9* morpholino (MO1) (Volkman et al., 2010). We found the proportion of mutant *hi2217* larvae characterized by epithelial extrusions at the yolk sac extension was reduced when *mmp9* was depleted (Fig. 2C). A similar reduction was observed with double injection of *mmp9* MO1 and *hai1* MO (Fig. 2C), suggesting that overexpression of

mmp9 contributes to the hyper-inflammation and epithelial defects in *hai1*-deficient larvae.

To investigate whether Mmp9 also contributes to neutrophil infiltration of the epithelium in the *hai1* mutants, we performed Sudan Black staining (Le Guyader et al., 2008) and quantified neutrophils outside of the caudal hematopoietic tissue (CHT). The *hai1* morphants co-injected with *mmp9* MO1 had significantly fewer neutrophils outside of the CHT compared with siblings injected with the *hai1* MO alone (Fig. 2A,D), indicating that Mmp9 depletion partially rescues neutrophil infiltration into the epithelium of *hai1*-deficient larvae. To confirm that the *mmp9* MO reduced Mmp9 activity, we utilized a recently reported MMP activity assay in zebrafish (Hall et al., 2014). Depletion of *hai1* was associated with increased MMP activation in the fin compared with control larvae (Fig. 2E). We rescued the increased MMP activity in *hai1* morphants by performing dual injection of *hai1* and *mmp9* MOs (Fig. 2E). Together, these data indicate that Mmp9 mediates neutrophilic infiltration and epithelial defects in *hai1*-deficient larvae.

SHG imaging reveals Mmp9-dependent collagen remodeling in the *hai1* morphants

It is known that Mmp9 alters the ECM through the cleavage of matrix components, including collagen (Collier et al., 1988; O'Farrell and Pourmotabbed, 2000; Van den Steen et al., 2002). To determine whether Mmp9 modulates the collagen matrix in *hai1* morphants we performed SHG imaging (Campagnola et al., 2002; Mohler et al., 2003). SHG imaging (Fig. 3A) is a label-free microscopy technique that exploits the interaction of light with ordered biological structures to visualize endogenous proteins, such as fibrillar collagen types I and III. Embryos injected with either control MO, *hai1* MO, *mmp9* MO1 or co-injected with *hai1* MO and *mmp9* MO1 at the one-cell stage were fixed at 3 dpf for SHG imaging (Fig. 3B). Single-blind analysis
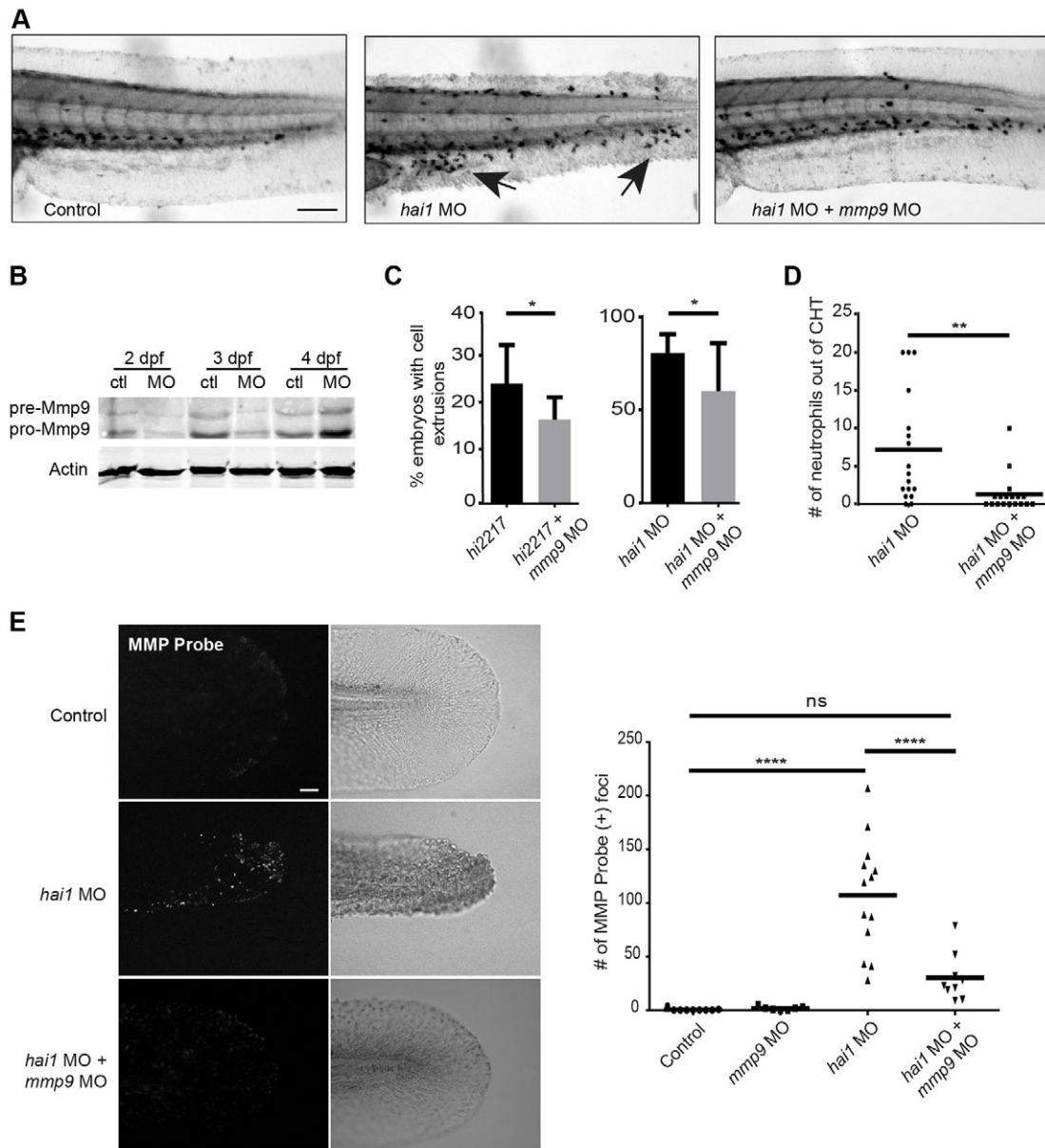
DEVELOPMENT

Fig. 2. Inflammatory phenotypes associated with *hai1* mutants are partially rescued by knockdown of *mmp9*. (A) Sudan Black staining of the *hai1* mutants show increased neutrophilic infiltration of the epithelium (arrows), a phenotype that could be rescued by *mmp9* knockdown. (B) Western blot analysis of *mmp9* MO1. (C) Morpholino knockdown of *mmp9* (MO1) decreased the proportion of *hi2217* and *hai1* morphants displaying epithelial extrusions and (D) decreased the number of neutrophils infiltrating the epithelium in the *hai1* morphants. (E) MMPSense showed hyper-activation of MMPs in the *hai1* morphants. Hyper-activation of MMPs in the *hai1* morphants could be partially rescued by the knockdown of *mmp9* expression (MO1). *$P<0.05$, **$P<0.01$ and ****$P<0.0001$. Scale bars: 300 µm in A; 40 µm in E. C and D represent data from a single experiment performed in triplicate.

of fiber organization on pooled and randomized images was performed ($\kappa=0.78$). Each image was scored from 1 to 3, with 1 representing fibers that are aligned and 3 representing fins with unaligned fibers (Fig. 3C). Analysis revealed that *hai1* morphants display a significant increase in the proportion of fins with unaligned fibers compared with control (Fig. 3D), a phenotype that could be partially rescued by co-injection of *mmp9* MO1 (Fig. 3D). Thus, Mmp9 appears to influence the arrangement of collagen fibers in the fins of *hai1* morphants (supplementary material Movies 1-3). Slight changes in collagen fiber alignment were also observed in a small number of *mmp9* morphants and are thought to be the result of minor unresolved abrasions due to the lack of Mmp9. As SHG is only sensitive to fibrillar collagen types

(Mohler et al., 2003), we also performed immunohistochemistry (IHC) to visualize non-fibrillar type IV collagen. Using IHC we did not observe any obvious differences in collagen organization or structure in the *hai1* morphants compared with control (Fig. 3E). Taken together, our data suggest that the alignment of collagen fibers is altered in *hai1* morphants, at least in part due to the overexpression of *mmp9*.

Mmp9 influences early leukocyte recruitment during caudal fin wound healing

Previous studies have shown that caudal fin amputation leads to increased expression of *mmp9* at the wound edge (Yoshinari et al., 2009). To determine whether the wounded epithelium was a
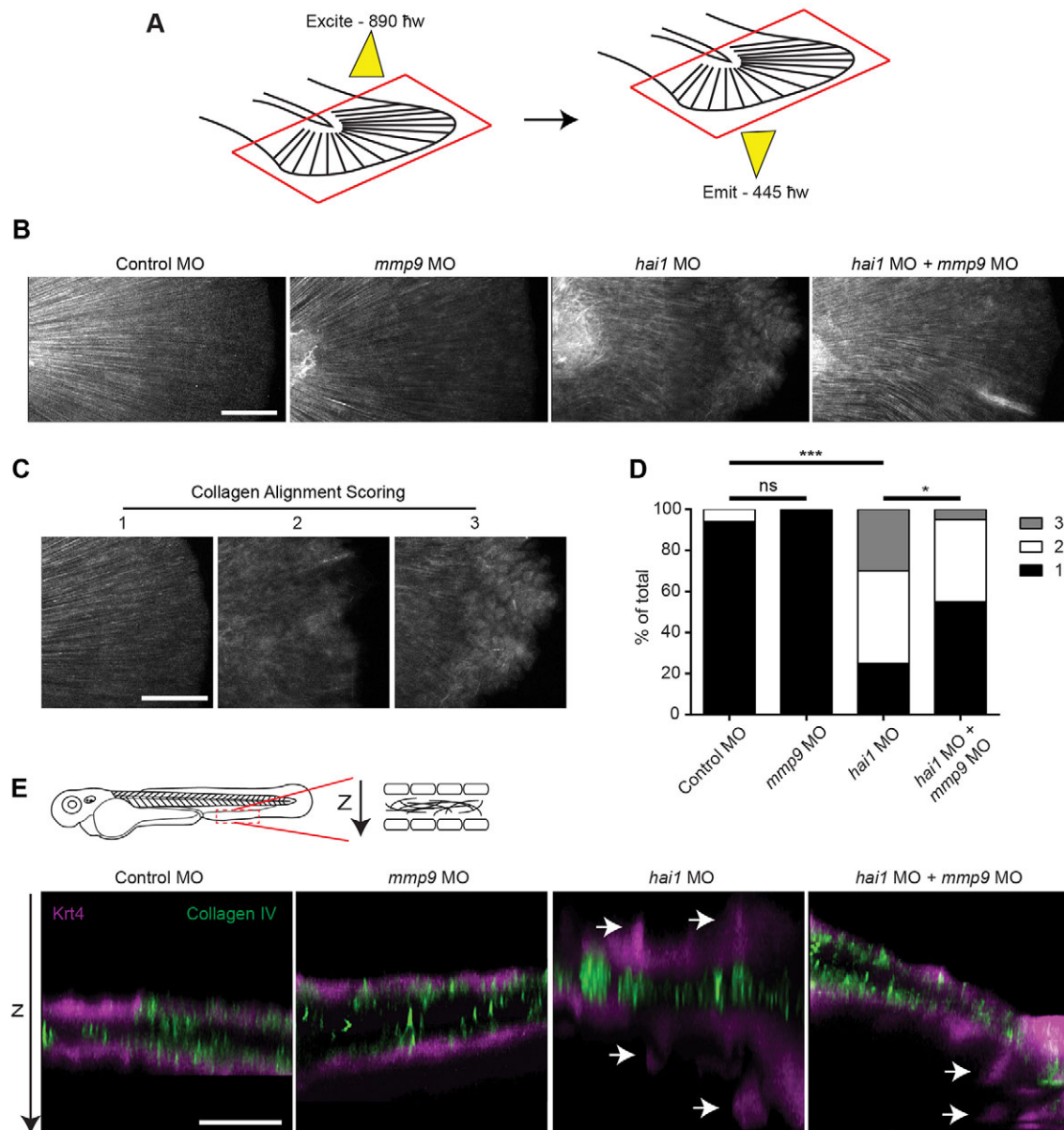
Fig. 3. SHG imaging shows altered collagen alignment in *hai1* morphants that is partially rescued by *mmp9* depletion. (A) SHG imaging of type I/III collagen. Caudal fins were excited with an 890 ℏw laser and collagen was detected at 445 ℏw. (B) Representative *z*-projected images of stitched multiple ROI SHG *z*-stacks. The *hai1* morphants display irregular collagen alignment. (C) In order to quantify alignment, SHG images illustrate scoring scheme, ranking severity of collagen mis-alignment for analysis from 1 to 3. (D) The *hai1* morphants display a significant decrease in collagen alignment that could be partially rescued upon knockdown of *mmp9* expression (MO1). (E) IHC of type IV collagen in the transgenic zebrafish Tg(*krt4:tdTom*). Epithelial extrusions were observed (arrows) in the *hai1* morphants. Knockdown of *mmp9* resulted in fewer observed extrusions. *$P<0.05$ and ***$P<0.001$. Scale bars: 50 µm in B,C; 20 µm in E. D represents the data from experiments performed in quadruplicate and scored by an individual, single-blind analyzer. D represents pooling with experimental numbers for Control MO=18, *mmp9* MO=18, *hai1* MO=20, *hai1* MO+*mmp9* MO=20.

source of the increased *mmp9* expression, we utilized a transgenic zebrafish, Tg(*kr4:l10a-gfp*), which labels the ribosomal subunit *l10a* in keratinocytes, and performed translating ribosomal affinity purification (TRAP) (Lam et al., 2013). At 6 h post-wounding (hpw), a significant increase in *mmp9* expression in epithelial cells was observed (Fig. 4A). To determine whether Mmp9 alters leukocyte recruitment to acute injury, as we found with the *hai1* mutant, we performed caudal fin transection. Mmp9-deficient larvae have an early impairment of macrophage recruitment at 1, 6 and 12 hpw, although resolution was not affected (supplementary material Fig. S2A). Similarly, the *mmp9* morphants displayed a significant reduction in the number of neutrophils recruited to the site of wounding at 1 hpw, as assessed

by Sudan Black staining (supplementary material Fig. S2B). Total neutrophil counts were performed on Mmp9-deficient larvae at 2 dpf and a significant reduction in the total number of neutrophils was observed (supplementary material Fig. S2C). However, no increase in neutrophil retention at the wound was observed at 24 or 48 hpw, indicating that Mmp9 depletion did not affect resolution of neutrophil inflammation at wounds.

Macrophage recruitment and function are required for complete regeneration in multiple models (Li et al., 2012; Lieschke et al., 2001; Martin et al., 2003; Petrie et al., 2014; van Furth et al., 1985). To determine whether the early reduction in macrophage presence alters regeneration in our system we performed morpholino
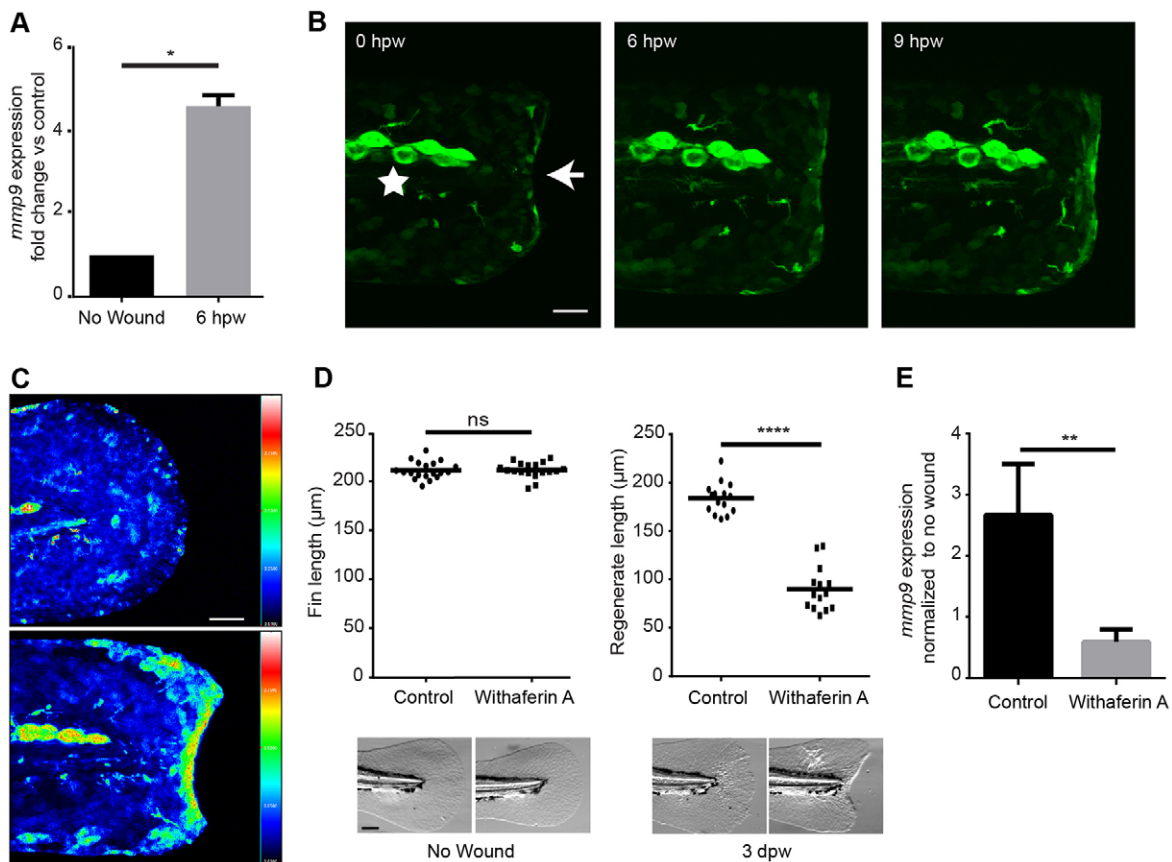
Fig. 4. Acute wounding induces NFκB-dependent expression of *mmp9*. (A) An increased expression of *mmp9* is observed by 6 h post wounding (hpw) in the 2-dpf embryo. (B) A visible increase in NFκB activation is seen by 6 hpw using the transgenic Tg(*NFκB:gfp*). The star denotes neuromast cells expressing high levels of gfp independent of wounding. The arrow indicates the edge of the wounded caudal fin and the site of increased NFκB activation. (C) Ratiometric image analysis performed in a cross of Tg(*NFκB:gfp*) and Tg(*krt4:tdTom*). (D) Early inhibition of the NFκB pathway with 30 μM withaferin A resulted in a significant reduction in regeneration at 3 dpw but had no effect on developmental fin length. (E) Early inhibition of the NFκB pathway resulted in an abrogation of the increased *mmp9* expression in the Tg(*krt4:l10a-gfp*) TRAP line. *$P<0.05$, **$P<0.01$ and ****$P<0.0001$. Scale bars: 40 μm in B,C; 100 μm in D. A represents data combined from experiments performed in triplicate; D represents data combined from experiments performed in quadruplicate and normalized to unwounded treatments.

knockdown of the transcription factor Irf8, which has been used to deplete macrophages with a concomitant increase in neutrophils (Li et al., 2011). Following caudal fin amputation, the *irf8* morphants displayed no defect in regenerate length at 3 days post-wounding (dpw) (supplementary material Fig. S2D). To further validate this result we targeted the Pu.1 transcription factor by morpholino, which blocks the development of both neutrophils and macrophages. The Pu.1-deficient embryos displayed no defect in caudal fin regeneration at 3 dpw (supplementary material Fig. S2D), consistent with a previous study using Pu.1 knockdown in larval zebrafish (Mathew et al., 2007). These findings indicate that the early leukocyte recruitment defect in Mmp9-deficient larvae is unlikely to affect regeneration at 3 dpw.

NFκB signaling mediates *mmp9* expression following caudal fin amputation

We took a candidate approach to identify the upstream signaling pathways that mediate wound-induced expression of *mmp9* (Fig. 1B and Fig. 4A). NFκB is a known regulator of *mmp9* expression in other systems (Eberhardt et al., 2002; Ganguly et al., 2013). Using a previously published NFκB reporter line, Tg(*NFκB:gfp*), we observed an increase in NFκB activity after tail transection by 6 hpw (Fig. 4B) (Kanther et al., 2011). Ratiometric imaging was performed by crossing the NFκB reporter with the keratinocyte-labeled transgenic Tg(*krt4:*

tdTom), and confirmed an increase in reporter activity after tail transection (Fig. 4C). This is in agreement with a recent report that identified increased NFκB activity after wounding in zebrafish larvae downstream of wound-induced H_2O_2 (Candel et al., 2014; de Oliveira et al., 2014). Because early wound signals like H_2O_2 have been shown to modulate regeneration (Yoo et al., 2012), we sought to determine whether NFκB activation was required for *mmp9* expression. Using a pharmacological inhibitor of the NFκB pathway, withaferin A, we found that early NFκB inhibition impaired caudal fin wound healing at 3 dpw (Fig. 4D). To determine whether the activation of NFκB was driving the expression of *mmp9* in the epithelium, we performed TRAP to isolate mRNA from control and NFκB-inhibited larvae. Pharmacological inhibition of NFκB was sufficient to block the increase in *mmp9* expression as quantified by qRT-PCR (Fig. 4E). Taken together, our findings suggest that NFκB signaling mediates the expression of *mmp9* following caudal fin amputation.

Wound-induced changes to collagen fibers are mediated by Mmp9

To determine whether Mmp9 also mediates changes to collagen matrices during acute injury we performed IHC and SHG imaging to visualize collagen organization following acute wounding. No clear changes in type IV collagen were observed by IHC after wounding (supplementary material Fig. S3A). By contrast, SHG
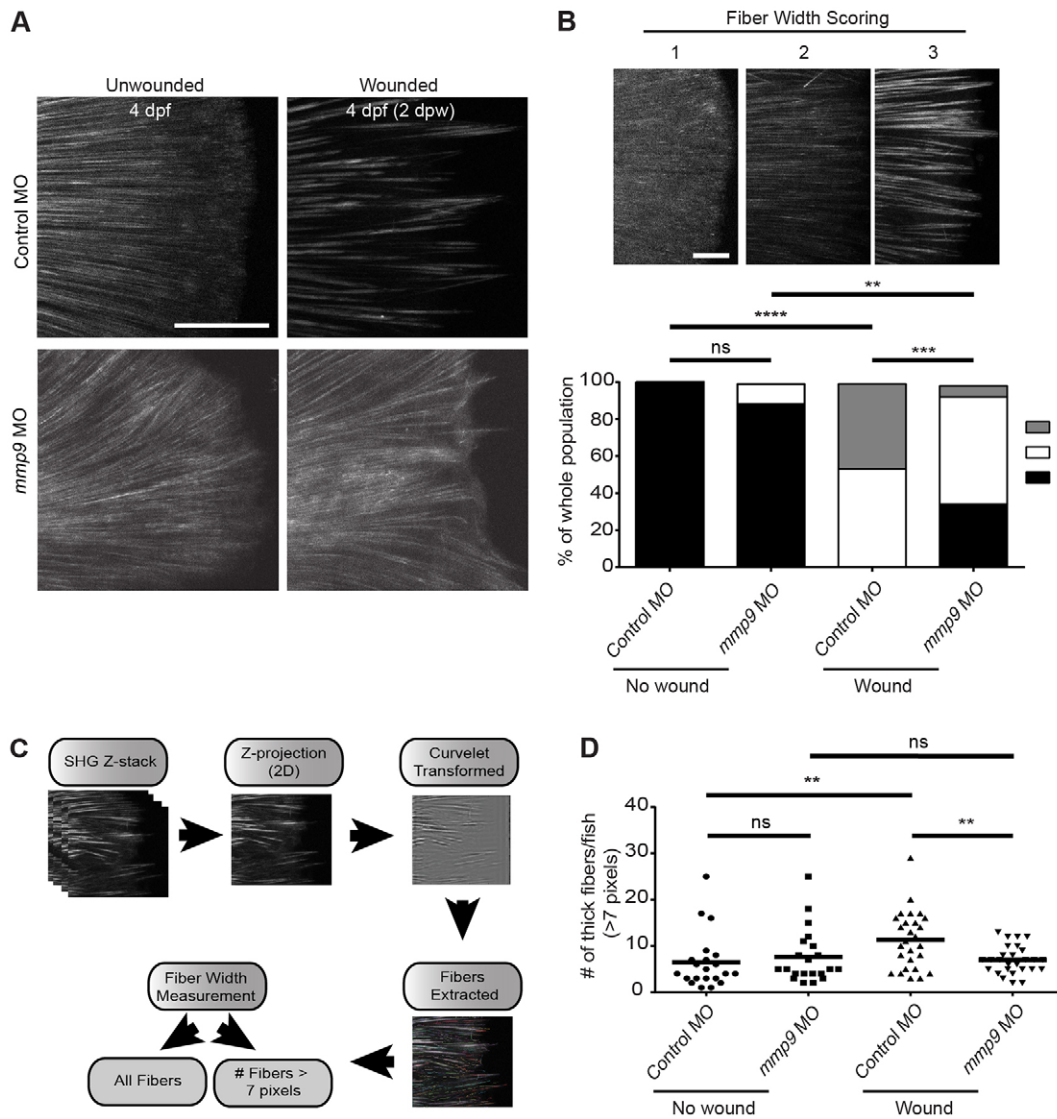
Fig. 5. SHG imaging reveals a defect in collagen thickening in the caudal fin of *mmp9* morphants at 2 days post amputation. (A) Amputation of the larval caudal fin results in a thickening of type I/III collagen fibers by 2 dpw (top). Fiber thickening does not appear to occur in the *mmp9* morphants (MO1) by 2 dpw (bottom). (B) Scoring system for fiber width, from 1 to 3 (top). A significant defect in collagen fiber thickness is seen in the *mmp9* morphants at 2 dpw (bottom). (C) Schematic illustrating the quantification of SHG images. All fibers were measured and the number of fibers above a given threshold width (i.e. 7 pixels) can be determined, see Materials and Methods. (D) Quantification of the number of fibers >7 pixels in diameter per caudal fin validates a defect in collagen fiber thickening in the *mmp9* morphants at 2 dpw. **$P<0.01$, ***$P<0.001$ and ****$P<0.0001$. Scoring in B from a single-blind analyzer from pooled experiments performed in triplicate. Data in D are from experiments performed in quadruplicate and scored by a single-blind analyzer. Scale bars: 50 µm in A; 20 µm in B. Experimental numbers for B and D: no wound Control MO=21, no wound *mmp9* MO=25, wounded Control MO=31, wounded *mmp9* MO=32.

imaging after tail transection revealed a significant increase in collagen fiber width during wound healing by 2 dpw (Fig. 5A). The increase in fiber width was not observed in unwounded age-matched controls (Fig. 5A). We depleted *mmp9* using morpholino to determine whether Mmp9 mediated this change. The Mmp9-deficient larvae had impaired fiber thickening at 2 dpw compared with control, suggesting that Mmp9 is involved in wound-induced fiber thickening (Fig. 5A). To quantify the change in fiber thickness we performed two forms of analysis. We used both single-blind fiber-width scoring (κ=0.58) (Fig. 5B) and a computational measurement of fiber thickness (Fig. 5C). Both methods of analysis revealed a significant increase in fiber width at 2 dpw in control animals that was impaired in Mmp9-deficient wounded larvae (Fig. 5B,D). Fiber alignment was also analyzed, but we found no statistical difference between wounded control and

Mmp9-deficient groups (supplementary material Fig. S3B). These data indicate that caudal fin amputation leads to a thickening of collagen fibers through an Mmp9-dependent mechanism.

Mmp9 is necessary for optimal caudal fin wound healing
The zebrafish caudal fin is known to undergo complete epimorphic regeneration following amputation (Poss et al., 2003) and we sought to determine whether the defect in collagen remodeling in the Mmp9-deficient embryos was associated with a deficit in caudal fin wound healing. We depleted *mmp9* expression (MO 1 and 2) and found that Mmp9-deficient larvae had impaired regenerate length (Fig. 6A; supplementary material Fig. S4A), indicating that Mmp9 is necessary for proper wound healing. The Mmp9 dependency was wound specific, as unwounded morphants did not display a defect in fin length compared with age-matched controls (Fig. 6A; supplementary material
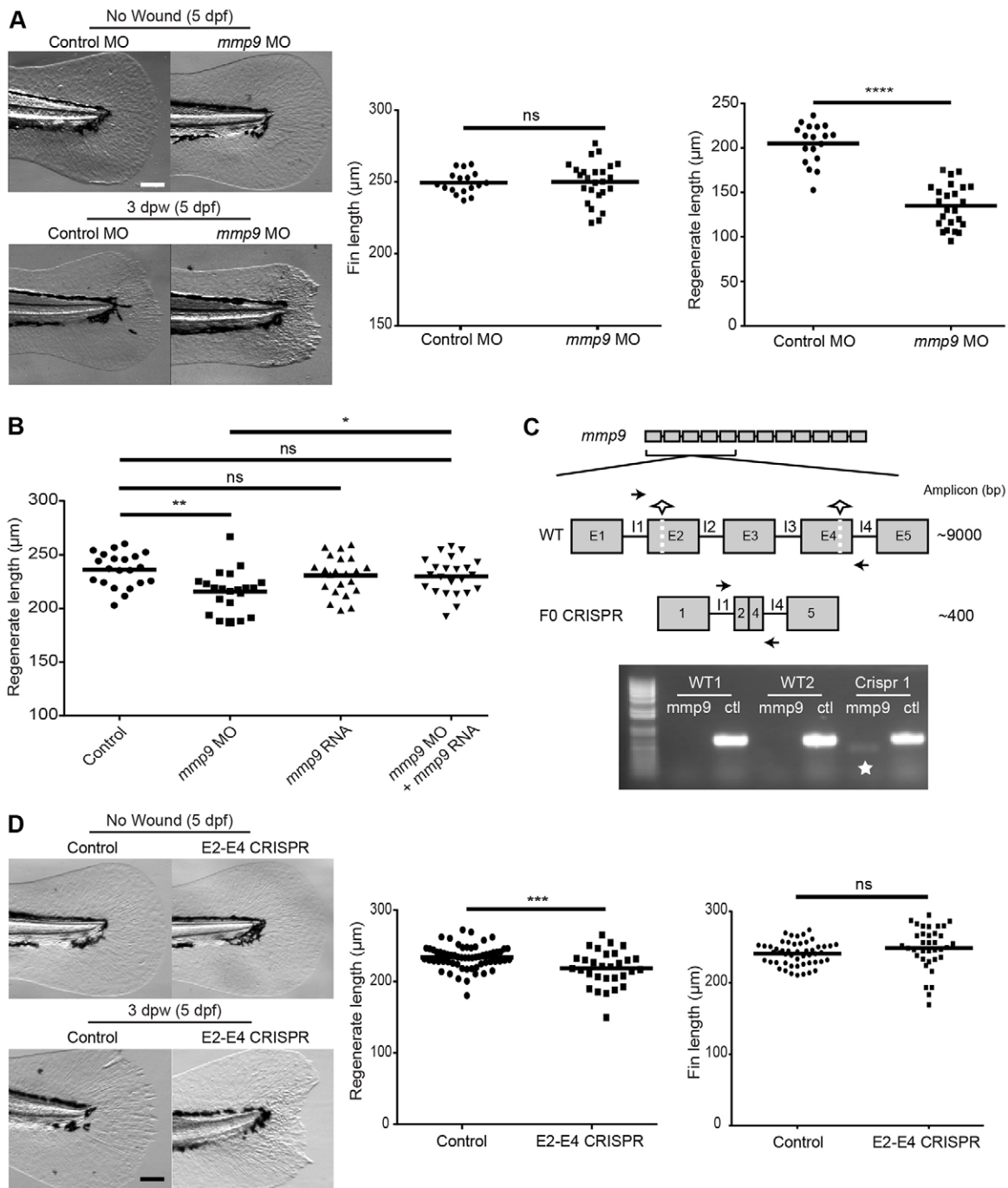
Fig. 6. Mmp9 regulates caudal fin wound healing following amputation. (A) Morpholino knockdown of *mmp9* (MO1) causes a regenerative defect at 3 dpw without influencing developmental fin length. (B) Co-injection of *mmp9* MO2 and zebrafish *mmp9* RNA (125 ng/µl) rescues the healing defect at 3 dpw (5 dpf). (C) Schematic of two-site CRISPR-Cas9 targeting of *mmp9* (top). Half-stars indicate CRISPR sites and arrows represent primer binding for screening. PCR amplification results in the presence of a ~400 bp amplicon indicated by the star, with the ctl lane representing a housekeeping gene to ensure the presence of gDNA (bottom). (D) Mosaic F0 larvae did not have altered fin lengths at 5 dpf but displayed a significant defect in caudal fin wound healing. *$P<0.05$, **$P<0.01$, ***$P<0.001$ and ****$P<0.0001$. Graphs represent a single experiment performed in triplicate. Scale bars: 100 µm in A,D.

Fig. S4A). To confirm that the regeneration defect was not due to off-target effects of MO, we rescued *mmp9* expression using co-injection of *mmp9* MO and zebrafish *mmp9* RNA. Co-injection of *mmp9* RNA rescued the regeneration defect of the morphants, supporting a requirement for Mmp9 during acute wound healing (Fig. 6B).

To further confirm a role for Mmp9 in acute wound healing, we utilized a two-cut CRISPR-Cas9 mutagenesis technique to create mosaic F0 *mmp9* mutants. In short, two separate exon targets were

identified (exon 2 and exon 4). Co-injection at the one-cell stage resulted in excision of a ~9000 bp segment of the *mmp9* genomic DNA (Fig. 6C) in a mosaic fashion in the developing larvae. At 2 dpf or at the completion of an experiment, genomic DNA was isolated from individual larvae and PCR screened for the presence of a ~400 bp segment to identify F0 mutant embryos (Fig. 6C). The amplicon was then purified and sequenced for further confirmation (supplementary material Fig. S4B). We found that the mosaic F0

DEVELOPMENT

mutants displayed a regeneration defect at 3 dpw (Fig. 6D) but had no effect on unwounded fin length (Fig. 6D). Taken together, these findings suggest that Mmp9 is necessary for acute wound healing and regeneration in the zebrafish larvae.

DISCUSSION

Here, we have demonstrated that Mmp9 plays important roles in acute and chronic tissue damage. In both cases, Mmp9 is involved in the infiltration of leukocytes; however, in the case of *hai1*-deficient larvae and chronic inflammation, Mmp9 contributed to abnormal collagen matrix composition and epidermal morphology. By contrast, in acute tissue damage associated with tail transection, Mmp9 was necessary for wound resolution and regeneration. Taken together, these findings suggest that a balance in Mmp9 activity is essential for normal tissue homeostasis and repair.

Resolution of inflammation is an essential step during wound repair (Starnes and Huttenlocher, 2012). In some human diseases, like pyoderma gangrenosum, inflammation fails to resolve, contributing to chronic wounds and tissue damage (Powell et al., 1985). These types of inflammatory disorders suggest that a tightly regulated inflammatory response is crucial to ensure proper wound healing (Eming et al., 2007) and that inflammation can contribute to compromised wound repair. However, substantial evidence indicates that leukocyte response to acute damage can be essential for the normal healing process (LeBert and Huttenlocher, 2014). Leukocyte recruitment is necessary to limit infection at the site of tissue damage (Nathan, 2006), and macrophage recruitment is required for optimal wound healing through the clearance of cellular debris (Leibovich and Ross, 1975; Li et al., 2012; Martin et al., 2003; Shiratori et al., 1996; Tidball and Wehling-Henricks, 2007; van Furth et al., 1985). Support for an important role for macrophages in wound repair has also been shown during regeneration in both larval zebrafish (Li et al., 2012) and the adult fin (Petrie et al., 2014).

Our findings suggest that increased *mmp9* expression regulates leukocyte infiltration to the inflammatory site, as depletion of *mmp9* impaired leukocyte recruitment in the context of both early acute inflammation and chronic tissue damage. This is in accordance with recent reports that suggest that Mmp9 promotes leukocyte recruitment to wounds (Hall et al., 2014; Parks et al., 2004). Interestingly, depletion of leukocytes (*pu.1* morpholino) or macrophages specifically (*irf8* morpholino) did not impair regeneration after tail transection. This agrees with recent data suggesting that the absence of macrophages impairs regeneration in adult zebrafish but does not result in a defect in wound repair in the larval zebrafish until 120 hpw (Petrie et al., 2014). Thus, our findings suggest that the defect in regeneration observed in Mmp9-deficient larvae was unlikely to be due to a defect in macrophage recruitment.

Mmp9 is known to have an essential role in remodeling the ECM, in particular through the proteolysis of specific targets like collagen IV (Collier et al., 1988). Using SHG imaging, we found that Mmp9 modulated the collagen organization in the context of both acute and chronic tissue damage. In the chronic injury model, with the *hai1* morphants, collagen fibers were characterized by poor organization; depletion of *mmp9* in these *hai1* morphants partially restored collagen fiber alignment, suggesting that Mmp9 contributes to the abnormal collagen architecture in the mutants. However, it is not clear whether this was due to a direct effect of Mmp9 on matrix organization or indirectly through its effects on epithelial cells, fibroblasts or leukocytes. As SHG only detects fibrillar collagen types such as I and III and not non-fibrillar collagen IV, it seems

likely that the effects are indirect. Regardless of the mechanism, the observation that depletion of *mmp9* partially rescues the altered collagen organization in the mutant suggests that Mmp9 plays a role in regulating ECM architecture in the context of chronic tissue damage.

To determine whether Mmp9 also affects collagen reorganization induced by acute wounding, we performed SHG imaging after tail transection. Surprisingly, SHG imaging after acute injury did not reveal changes to collagen fiber alignment as was observed in the chronic injury model. Instead, acute wounding induced a thickening of collagen fibers in the larval fin. Interestingly, the fiber thickening induced by acute injury was dependent upon *mmp9* expression, as morphants did not show wound-induced collagen fiber thickening. Taken together, these findings suggest that Mmp9 mediates the changes in collagen fiber organization that occur in both acute and chronic tissue damage. However, in the case of chronic injury, Mmp9 has detrimental effects, whereas, with acute injury, Mmp9 mediates the changes in collagen fiber organization that are part of the normal repair process.

In the current study we show that Mmp9 regulates collagen structure after wounding. However, as of yet, we do not know the significance of the fiber thickening that occurs after acute injury. In future studies it will be informative to perform live imaging of fiber architecture over time to determine whether Mmp9 regulates the transition in fiber thickness as wound healing progresses. It is known that, following injury in mammalian models, surrounding fibroblasts rapidly produce collagen (Eickelberg et al., 1999; Yates et al., 2012), providing a transient matrix for stability. The type of collagen produced appears to be age dependent and coincides with whether a wound scars or regenerates. Adult wound-induced ECM is predominately the thicker type I collagen, whereas fetal wound-induced collagen is the thinner type III collagen (Yates et al., 2012). SHG imaging does not discriminate between type I and III collagen, and it is therefore possible that Mmp9 is involved in a switch in collagen type during repair. Taken together, our findings demonstrate that Mmp9 promotes acute wound resolution and collagen fiber remodeling, and supports the idea that proper regulation of Mmp9 is required to prevent the progression towards chronic tissue damage and inflammation.

MATERIALS AND METHODS
Zebrafish maintenance and handling
All protocols using zebrafish in this study were approved by the University of Wisconsin-Madison Research Animals Resource Center. Adult zebrafish and embryos were maintained as described previously (Yoo et al., 2010). For wounding assays, 2-dpf larvae were anesthetized in E3 containing 0.2 mg/ml tricaine (ethyl 3-aminobenzoate; Sigma-Aldrich). To prevent pigment formation, some larvae were maintained in E3 containing 0.2 mM *N*-phenylthiourea (Sigma-Aldrich).

Microarray design and analysis
Adults heterozygous for the *hi2217* retroviral insertion in the *hai* locus (Mathias et al., 2007) were crossed and RNA samples were extracted from WT siblings or *hi2217* homozygous mutants. Adults heterozygous for the *hi1520* retroviral insertion within the *clint1* locus (Dodd et al., 2009) were crossed and RNA samples from WT sibling and *hi1520* mutants were collected. Pools of 30-50 embryos of WT siblings and *hi2217* or *hi1520* mutants were collected at 3 dpf for RNA isolation. Embryos were homogenized in RNA Stat60 (Teltest). RNA was purified using standard chloroform phase separation, isopropanol precipitation and ethanol wash steps. RNA from the *hi2217* or *hi1520* mutant embryos was labelled with Cy5 and hybridized against Cy3-labeled RNA from the corresponding WT sibling embryos. Experiments were performed in triplicate. RNA isolation, synthesis of amino allyl-labeled aRNA, dye coupling and hybridization

conditions were as previously described (Stockhammer et al., 2009). Microarray analysis was performed using custom-designed 44-k Agilent chips (GEO platform accession: GPL7735), described elsewhere (Stockhammer et al., 2009). Microarray data were processed and analyzed as described (Zakrzewska et al., 2010). Significance cut-offs for differentially expressed probe sequences were set at 1.5-fold change at $P<10^{-5}$. The data were submitted to the GEO database (www.ncbi.nlm.nih.gov/geo) and are available under accession number GSE28110.

Regeneration assays

For regeneration assays, tail transection was performed on 2- to 2.5-dpf larvae using a surgical blade (Feather, no. 10). Regenerate length was quantified by measuring the distance between the caudal tip of the notochord and the caudal tip of the tail fin at 3 dpw. Withaferin A (Tocris) treatment for 1 h before and after wounding at 30 µM was performed to pharmacologically inhibit NFκB activity.

Immunofluorescence and Sudan Black staining

Larvae (2.5-3.5 dpf) were fixed with 1.5% paraformaldehyde in 0.1 M Pipes (Sigma-Aldrich), 1.0 mM $MgSO_4$ (Sigma-Aldrich) and 2 mM EGTA (Sigma-Aldrich) overnight at 4°C and immunolabeled as previously described (Yoo and Huttenlocher, 2011). The following primary antibody was used: rabbit anti-collagen type IV (PAb, Ab6586; Abcam) at 1:300. Dylight 488- or 549-conjugated mouse anti-rabbit IgG antibodies (Jackson ImmunoResearch Laboratories, 211-482-171, 211-502-171) were used as secondary antibodies at 1:250. Immunofluorescence images were acquired with a confocal microscope (FluoView FV1000; Olympus) using a NA 0.75/20× objective. Each fluorescence channel was acquired by sequential line scanning. Z-series were acquired using 180- to 280-µm pinhole and 0.5- to 5-µm step sizes. Z-series images were stacked or three-dimensionally (3D) reconstructed by the FluoView FV1000 software. For Sudan Black staining, embryos (1, 6, 24, 48 h after wounding) were fixed in 4% paraformaldehyde in PBS overnight at 4°C, rinsed in PBS and incubated in 0.03% Sudan Black, followed by extensive washing in 70% ethanol. After rehydration in PBST, pigments were removed by incubation in a 1% H_2O_2 (Fisher Scientific) and 1% KOH (Sigma-Aldrich) solution. Embryos were observed using a stereoscopic zoom microscope (SMZ1500; Nikon). To image MMP activity, we used MMPSense 645 FAST (PerkinElmer, NEV10100, absorption/emission maxima of 649/666), following a previously established protocol (Hall et al., 2014). Immunofluorescence images were acquired with a confocal microscope (FluoView FV1000; Olympus) using a NA 0.75/20× objective.

Ratiometric image analysis

Images were acquired with a confocal microscope (FluoView FV1000; Olympus) using a NA 0.75/20× objective and performing sequential line scanning. Ratiometric analysis was performed by using FluoView FV1000 software. Two-dimensional (2D) ratiometric images were created after z-series stacking. After complete loss of background by subtraction in the numerator channel, ratio images were created by dividing the numerator channel with the denominator channel and processed by a median filter to remove background noise.

Translating ribosome affinity purification (TRAP)

TRAP was performed as described previously (Lam et al., 2013). Pools of 30-50 3-dpf Tg(krt4:l10a-gfp) larvae were collected for each condition. RNA was purified using the miRvana RNA purification kit (Ambion) and eluted in 30-50 µl of nuclease-free water (Ambion).

Whole-embryo RNA extraction for qRT-PCR

RNA was extracted from whole embryos using the miRvana RNA purification kit (Ambion). One-step qRT-PCR was performed in triplicate using Super Script III Platinum SYBR Green (Invitrogen) from purified TRAP or whole-embryo RNA. Fold change was determined using efficiency-corrected comparative quantitation. Data were normalized to control samples.

Primers: Ef1α: F – 5′-TGCCTTCGTCCCAATTTCAG-3′, R – 5′-TACCCTCCTTGCGCTCAATC-3′; Mmp9: F – 5′-TGATGTGCTTGGACCACGTAA-3′, R – 5′-ACAGGAGCACCTTGCCTTTTC-3′; Il-1β: F – 5′-CACATTTGAAGGCCGTCACACT-3′, R – 5′-CTCGGCGGGGCAACAGG-3′; Tnf-β: F – 5′-CCTCAGACCACGGAAAAGT-3′, R – 5′-GCCCTGTTGGAATGCCTGAT-3′; Mmp13: F – 5′-AAGGAATAAGGCAAATGGATAAAG-3′, R – 5′-TTTGATCCACTGAAGAGGTA-3′; Myd88: F – 5′-GTGTAAGAGGATGGTGGTG-3′, R – 5′-GTAGACGACAGGGATTAGC-3′.

Morpholino injections

Morpholino oligonucleotides (Gene Tools) were re-suspended in water to a stock concentration of 1 mM. Final morpholino concentrations were injected into one- to two-cell stage embryos in 3-nl amounts and embryos were maintained at 28.5°C. Morpholino sequences used have been previously described as follows: mmp9 MO1 (Volkman et al., 2010), mmp9 MO2 (Hall et al., 2014), pu.1 MO (Rhodes et al., 2005), hai1 splice-blocking MO (Mathias et al., 2007) and irf8 MO (Li et al., 2011); control MO: 5′-CCTCTTACCTCAGTTACAATTTATA-3′.

In situ hybridization

A plasmid (pcs2.1, Invitrogen) containing mmp9 was grown and harvested (Maxi-prep, Clontech). The plasmid was linearized using restriction enzymes to serve as template for transcription of digoxigenin-labeled anti-sense probes using T3 RNA polymerase. Whole-mount in situ hybridization was performed as described on 2-dpf embryos (Jowett and Yan, 1996). Following staining, embryos were placed in 80% glycerol for microscopy. Pictures were recorded with a Nikon Digital Sight camera on the Nikon SMZ1500 microscope.

SHG imaging and processing

Tails were removed (~1- to 2-mm fragments) from the main body of fixed zebrafish embryos (so tail fins lay approximately flat) in a drop of PBS in a glass-bottomed imaging dish (Fluodishes, World Precision Instruments). Tails were imaged on a custom-built multiphoton microscope at the Laboratory for Optical and Computational Instrumentation (Conklin et al., 2009). Briefly, the microscope consists of a tunable titanium sapphire laser (Mira, Coherent) with an inverted microscope (TE2000, Nikon) driven by WiscScan software (http://loci.wisc.edu/software/wiscscan). For SHG imaging of the tails, a 40× water immersion lens (1.25 NA, Nikon) was used, the laser was tuned to 890 nm and backwards SHG was collected through a 445/20 emission filter and detected on a H7422 GaAsP photomultiplier tube (PMT) (Hamamatsu, Japan). Brightfield images were simultaneously collected in transmission mode with a photodiode-based detector (Bio-Rad). Imaging parameters were kept constant across all imaging days. Images were collected as z-stacks, with optical sections 1 µm apart, at 512×512 resolution. Images were collected from the tip of the notochord to the tip of the tail or to the wound site. A minimum of six tails per treatment per replicate were collected. Because the tail is three-dimensional and angled, for visualization and analyses sum projections of the image z-stacks were generated in FIJI (Schindelin et al., 2012). Sum projections were analyzed for fiber width using CT-FIRE software (Bredfeldt et al., 2014; 2. CT-FIRE | LOCI, available at http://loci.wisc.edu/software/ctfire) (see also Fig. 5C). Briefly, individual fibers were extracted from each projected image. The width of each fiber was calculated as the average width of the points automatically selected to represent the fiber as assessed by the algorithm in CT-FIRE. Using these width measurements, the number of fibers ≥7 pixels was determined for each projection.

Statistical analyses

Assuming a Gaussian distribution of the overall population of values, P-values were driven by two-tailed paired t-test (two comparisons) or one-way analysis of variance (ANOVA) (multiple comparisons) comparing means of each sample. Data are representative of at least three separate experiments. The single-blind SHG was analyzed using chi-squared test on data scored by a single scorer, pooled from all experiments. Reliability of single-blind analysis was assessed by determining the κ index.

Western blot

Approximately 60 embryos were collected at 2, 3 and 4 dpf, de-yolked and homogenized using a 1 ml Dounce homogenizer. Samples were sonicated five times for 3 s at 20% amplitude and centrifuged at 18,000 g for 10 min at 4°C. Samples were run on a 10% acrylamide gel and blocked with 5% milk/TS-T. The primary antibodies anti-Mmp9 at 1:250 (Abcam, ab38898) and anti-Actin at 1:2000 (Sigma-Aldrich, a5441) were used; for secondary antibodies, anti-rabbit 800 (Rockland, 611-131-122) and anti-mouse 600 (Invitrogen, A21057) were used at 1:1000. The blots were imaged with an infrared imaging system (Odyssey, LI-COR Biosciences).

CRISPR-Cas9

CRISPR guide RNAs were designed using the Joung Lab zifit site: http://zifit.partners.org/ZiFiT/Disclaimer.aspx.

Exon 2: Oligo1-TAGGTGGGCTGGTCAAGCAAGC, Oligo2-AAAC-GCTTGCTTGACCAGCCCA; Exon 4: Oligo1-TAGGTGATCCCTACC-CCTTTGA, Oligo2-AAACTCAAAGGGGTAGGGATCA.

The pT7 gRNA vector (Addgene 46759) was digested with *Bsm*BI, *Bgl*II and *Sal*I (New England Biolabs) and diluted to 5 ng/µl in ddH$_2$O. Annealed oligos were ligated into vector using quick ligase (New England Biolabs). Single colonies were selected following transformation and digest-confirmed with *Bgl*II. Candidate plasmids were sequenced using M13 primer. Sequence-confirmed plasmids were linearized with *Bam*HI (New England Biolabs) and *in vitro*-transcribed using MAXIScript T7 kit (Ambion, Life Technologies). The resulting guide RNAs were injected into the yolk at the one-cell stage at a volume of 2 nl. The final concentrations of the injection mixes were as follows: gRNAs at ~40 ng/µl and Cas9 protein (New England Biolabs) at ~55 ng/µl. To confirm, 2- to 5-dpf larval zebrafish were individually lysed in 50 µl of 50 mM NaOH at 95°C for 10 min. Samples were cooled to 4°C and mixed with 1 M Tris-HCl (pH 8.0). Supernatant was collected after 5 min, 2000 g centrifugation. PCR was performed on gDNA to confirm with the following primers for *mmp9*: intron 1 forward: 5′-GTTTGGGTTTCTCCTCTCGGTTCTCTA-CT-3′; intron 4 reverse: 5′-AACTGCAGAGGGAGCTATTGCTCCTC-3′.

References

Bai, S., Thummel, R., Godwin, A. R., Nagase, H., Itoh, Y., Li, L., Evans, R., McDermott, J., Seiki, M. and Sarras, M. P., Jr (2005). Matrix metalloproteinase expression and function during fin regeneration in zebrafish: analysis of MT1-MMP, MMP2 and TIMP2. *Matrix Biol.* **24**, 247-260.

Betsuyaku, T., Fukuda, Y., Parks, W. C., Shipley, J. M. and Senior, R. M. (2000). Gelatinase B is required for alveolar bronchiolization after intratracheal bleomycin. *Am. J. Pathol.* **157**, 525-535.

Bredfeldt, J. S., Liu, Y., Pehlke, C. A., Conklin, M. W., Szulczewski, J. M., Inman, D. R., Keely, P. J., Nowak, R. D., Mackie, T. R. and Eliceiri, K. W. (2014). Computational segmentation of collagen fibers from second-harmonic generation images of breast cancer. *J. Biomed. Opt.* **19**, 016007.

Campagnola, P. J., Millard, A. C., Terasaki, M., Hoppe, P. E., Malone, C. J. and Mohler, W. A. (2002). Three-dimensional high-resolution second-harmonic generation imaging of endogenous structural proteins in biological tissues. *Biophys. J.* **82**, 493-508.

Candel, S., de Oliveira, S., López-Muñoz, A., García-Moreno, D., Espín-Palazón, R., Tyrkalska, S. D., Cayuela, M. L., Renshaw, S. A., Corbalán-Vélez, R., Vidal-Abarca, I. et al. (2014). Tnfa signaling through tnfr2 protects skin against oxidative stress–induced inflammation. *PLoS Biol.* **12**, e1001855.

Carney, T. J., von der Hardt, S., Sonntag, C., Amsterdam, A., Topczewski, J., Hopkins, N. and Hammerschmidt, M. (2007). Inactivation of serine protease Matriptase1a by its inhibitor Hai1 is required for epithelial integrity of the zebrafish epidermis. *Development* **134**, 3461-3471.

Castaneda, F. E., Walia, B., Vijay-Kumar, M., Patel, N. R., Roser, S., Kolachala, V. L., Rojas, M., Wang, L., Oprea, G., Garg, P. et al. (2005). Targeted deletion of metalloproteinase 9 attenuates experimental colitis in mice: central role of epithelial-derived MMP. *Gastroenterology* **129**, 1991-2008.

Collier, I. E., Wilhelm, S. M., Eisen, A. Z., Marmer, B. L., Grant, G. A., Seltzer, J. L., Kronberger, A., He, C. S., Bauer, E. A. and Goldberg, G. I. (1988). H-ras oncogene-transformed human bronchial epithelial cells (TBE-1) secrete a single metalloprotease capable of degrading basement membrane collagen. *J. Biol. Chem.* **263**, 6579-6587.

Conklin, M. W., Provenzano, P. P., Eliceiri, K. W., Sullivan, R. and Keely, P. J. (2009). Fluorescence lifetime imaging of endogenous fluorophores in histopathology sections reveals differences between normal and tumor epithelium in carcinoma in situ of the breast. *Cell Biochem. Biophys.* **53**, 145-157.

de Oliveira, S., Lopez-Munoz, A., Candel, S., Pelegrin, P., Calado, A. and Mulero, V. (2014). ATP modulates acute inflammation in vivo through dual oxidase 1-derived H2O2 production and NF-kappaB activation. *J. Immunol.* **192**, 5710-5719.

Dodd, M. E., Hatzold, J., Mathias, J. R., Walters, K. B., Bennin, D. A., Rhodes, J., Kanki, J. P., Look, A. T., Hammerschmidt, M. and Huttenlocher, A. (2009). The ENTH domain protein Clint1 is required for epidermal homeostasis in zebrafish. *Development* **136**, 2591-2600.

Eberhardt, W., Schulze, M., Engels, C., Klasmeier, E. and Pfeilschifter, J. (2002). Glucocorticoid-mediated suppression of cytokine-induced matrix metalloproteinase-9 expression in rat mesangial cells: involvement of nuclear factor-kappaB and Ets transcription factors. *Mol. Endocrinol.* **16**, 1752-1766.

Eickelberg, O., Kohler, E., Reichenberger, F., Bertschin, S., Woodtli, T., Erne, P., Perruchoud, A. P. and Roth, M. (1999). Extracellular matrix deposition by primary human lung fibroblasts in response to TGF-beta1 and TGF-beta3. *Am. J. Physiol.* **276**, L814-L824.

Eming, S. A., Krieg, T. and Davidson, J. M. (2007). Inflammation in wound repair: molecular and cellular mechanisms. *J. Invest. Dermatol.* **127**, 514-525.

Feghali, C. A. and Wright, T. M. (1997). Cytokines in acute and chronic inflammation. *Front. Biosci.* **2**, d12-d26.

Fini, M. E., Parks, W. C., Rinehart, W. B., Girard, M. T., Matsubara, M., Cook, J. R., West-Mays, J. A., Sadow, P. M., Burgeson, R. E., Jeffrey, J. J. et al. (1996). Role of matrix metalloproteinases in failure to re-epithelialize after corneal injury. *Am. J. Pathol.* **149**, 1287-1302.

Fosang, A. J., Neame, P. J., Last, K., Hardingham, T. E., Murphy, G. and Hamilton, J. A. (1992). The interglobular domain of cartilage aggrecan is cleaved by PUMP, gelatinases, and cathepsin B. *J. Biol. Chem.* **267**, 19470-19474.

Ganguly, K., Rejmak, E., Mikosz, M., Nikolaev, E., Knapska, E. and Kaczmarek, L. (2013). Matrix metalloproteinase (MMP) 9 transcription in mouse brain induced by fear learning. *J. Biol. Chem.* **288**, 20978-20991.

Hall, C. J., Boyle, R. H., Sun, X., Wicker, S. M., Misa, J. P., Krissansen, G. W., Print, C. G., Crosier, K. E. and Crosier, P. S. (2014). Epidermal cells help coordinate leukocyte migration during inflammation through fatty acid-fuelled matrix metalloproteinase production. *Nat. Commun.* **5**, 3880.

Hattori, N., Mochizuki, S., Kishi, K., Nakajima, T., Takaishi, H., D'Armiento, J. and Okada, Y. (2009). MMP-13 plays a role in keratinocyte migration, angiogenesis, and contraction in mouse skin wound healing. *Am. J. Pathol.* **175**, 533-546.

Jowett, T. and Yan, Y.-L. (1996). Double fluorescent in situ hybridization to zebrafish embryos. *Trends Genet.* **12**, 387-389.

Kanther, M., Sun, X., Mühlbauer, M., Mackey, L. C., Flynn, E. J., III, Bagnat, M., Jobin, C. and Rawls, J. F. (2011). Microbial colonization induces dynamic temporal and spatial patterns of NF-kappaB activation in the zebrafish digestive tract. *Gastroenterology* **141**, 197-207.

Lam, P.-Y., Harvie, E. A. and Huttenlocher, A. (2013). Heat shock modulates neutrophil motility in zebrafish. *PLoS ONE* **8**, e84436.

Le Guyader, D., Redd, M. J., Colucci-Guyon, E., Murayama, E., Kissa, K., Briolat, V., Mordelet, E., Zapata, A., Shinomiya, H. and Herbomel, P. (2008). Origins and unconventional behavior of neutrophils in developing zebrafish. *Blood* **111**, 132-141.

LeBert, D. C. and Huttenlocher, A. (2014). Inflammation and wound repair. *Semin. Immunol.* **26**, 315-320.

Leibovich, S. J. and Ross, R. (1975). The role of the macrophage in wound repair. A study with hydrocortisone and antimacrophage serum. *Am. J. Pathol.* **78**, 71-100.

Li, L., Jin, H., Xu, J., Shi, Y. and Wen, Z. (2011). Irf8 regulates macrophage versus neutrophil fate during zebrafish primitive myelopoiesis. *Blood* **117**, 1359-1369.

Li, L., Yan, B., Shi, Y.-Q., Zhang, W.-Q. and Wen, Z.-L. (2012). Live imaging reveals differing roles of macrophages and neutrophils during zebrafish tail fin regeneration. *J. Biol. Chem.* **287**, 25353-25360.

Lieschke, G. J., Oates, A. C., Crowhurst, M. O., Ward, A. C. and Layton, J. E. (2001). Morphologic and functional characterization of granulocytes and macrophages in embryonic and adult zebrafish. *Blood* **98**, 3087-3096.

Martin, P., D'Souza, D., Martin, J., Grose, R., Cooper, L., Maki, R. and McKercher, S. R. (2003). Wound healing in the PU.1 null mouse – tissue repair is not dependent on inflammatory cells. *Curr. Biol.* **13**, 1122-1128.

Mathew, L. K., Sengupta, S., Kawakami, A., Andreasen, E. A., Lohr, C. V., Loynes, C. A., Renshaw, S. A., Peterson, R. T. and Tanguay, R. L. (2007). Unraveling tissue regeneration pathways using chemical genetics. *J. Biol. Chem.* **282**, 35202-35210.

Mathias, J. R., Dodd, M. E., Walters, K. B., Rhodes, J., Kanki, J. P., Look, A. T. and Huttenlocher, A. (2007). Live imaging of chronic inflammation caused by mutation of zebrafish Hai1. *J. Cell Sci.* **120**, 3372-3383.

McCarty, S. M. and Percival, S. L. (2013). Proteases and delayed wound healing. *Adv. Wound Care* **2**, 438-447.

McCawley, L. J., O'Brien, P. and Hudson, L. G. (1998). Epidermal growth factor (EGF)- and scatter factor/hepatocyte growth factor (SF/HGF)-mediated keratinocyte migration is coincident with induction of matrix metalloproteinase (MMP)-9. *J. Cell. Physiol.* **176**, 255-265.

Mohan, R., Chintala, S. K., Jung, J. C., Villar, W. V. L., McCabe, F., Russo, L. A., Lee, Y., McCarthy, B. E., Wollenberg, K. R., Jester, J. V. et al. (2002). Matrix metalloproteinase gelatinase B (MMP-9) coordinates and effects epithelial regeneration. *J. Biol. Chem.* **277**, 2065-2072.

Mohler, W., Millard, A. C. and Campagnola, P. J. (2003). Second harmonic generation imaging of endogenous structural proteins. *Methods* **29**, 97-109.

Nathan, C. (2006). Neutrophils and immunity: challenges and opportunities. *Nat. Rev. Immunol.* **6**, 173-182.

O'Farrell, T. J. and Pourmotabbed, T. (2000). Identification of structural elements important for matrix metalloproteinase type V collagenolytic activity as revealed by chimeric enzymes. Role of fibronectin-like domain and active site of gelatinase B. *J. Biol. Chem.* **275**, 27964-27972.

Parks, W. C., Wilson, C. L. and López-Boado, Y. S. (2004). Matrix metalloproteinases as modulators of inflammation and innate immunity. *Nat. Rev. Immunol.* **4**, 617-629.

Petrie, T. A., Strand, N. S., Tsung-Yang, C., Rabinowitz, J. S. and Moon, R. T. (2014). Macrophages modulate adult zebrafish tail fin regeneration. *Development* **141**, 2581-2591.

Poss, K. D., Keating, M. T. and Nechiporuk, A. (2003). Tales of regeneration in zebrafish. *Dev. Dyn.* **226**, 202-210.

Powell, F. C., Schroeter, A. L., Su, W. P. and Perry, H. O. (1985). Pyoderma gangrenosum: a review of 86 patients. *Q. J. Med.* **55**, 173-186.

Rhodes, J., Hagen, A., Hsu, K., Deng, M., Liu, T. X., Look, A. T. and Kanki, J. P. (2005). Interplay of pu.1 and gata1 determines myelo-erythroid progenitor cell fate in zebrafish. *Dev. Cell* **8**, 97-108.

Schindelin, J., Arganda-Carreras, I., Frise, E., Kaynig, V., Longair, M., Pietzsch, T., Preibisch, S., Rueden, C., Saalfeld, S., Schmid, B. et al. (2012). Fiji: an open-source platform for biological-image analysis. *Nat. Methods* **9**, 676-682.

Senior, R. M., Griffin, G. L., Fliszar, C. J., Shapiro, S. D., Goldberg, G. I. and Welgus, H. G. (1991). Human 92- and 72-kilodalton type IV collagenases are elastases. *J. Biol. Chem.* **266**, 7870-7875.

Shiratori, Y., Hongo, S., Hikiba, Y., Ohmura, K., Nagura, T., Okano, K., Kamii, K., Tanaka, T., Komatsu, Y., Ochiai, T. et al. (1996). Role of macrophages in regeneration of liver. *Dig. Dis. Sci.* **41**, 1939-1946.

Starnes, T. W. and Huttenlocher, A. (2012). Neutrophil reverse migration becomes transparent with zebrafish. *Adv. Hematol.* **2012**, 398640.

Stockhammer, O. W., Zakrzewska, A., Hegedus, Z., Spaink, H. P. and Meijer, A. H. (2009). Transcriptome profiling and functional analyses of the zebrafish embryonic innate immune response to Salmonella infection. *J. Immunol.* **182**, 5641-5653.

Tidball, J. G. and Wehling-Henricks, M. (2007). Macrophages promote muscle membrane repair and muscle fibre growth and regeneration during modified muscle loading in mice in vivo. *J. Physiol.* **578**, 327-336.

Van den Steen, P. E., Proost, P., Grillet, B., Brand, D. D., Kang, A. H., Van Damme, J. and Opdenakker, G. (2002). Cleavage of denatured natural collagen type II by neutrophil gelatinase B reveals enzyme specificity, post-translational modifications in the substrate, and the formation of remnant epitopes in rheumatoid arthritis. *FASEB J.* **16**, 379-389.

van Furth, R., Nibbering, P. H., van Dissel, J. T. and Diesselhoff-den Dulk, M. M. C. (1985). The characterization, origin, and kinetics of skin macrophages during inflammation. *J. Invest. Dermatol.* **85**, 398-402.

Vandooren, J., Van den Steen, P. E. and Opdenakker, G. (2013). Biochemistry and molecular biology of gelatinase B or matrix metalloproteinase-9 (MMP-9): the next decade. *Crit. Rev. Biochem. Mol. Biol.* **48**, 222-272.

Volkman, H. E., Pozos, T. C., Zheng, J., Davis, J. M., Rawls, J. F. and Ramakrishnan, L. (2010). Tuberculous granuloma induction via interaction of a bacterial secreted protein with host epithelium. *Science* **327**, 466-469.

Wyatt, R. A., Keow, J. Y., Harris, N. D., Haché, C. A., Li, D. H. and Crawford, B. D. (2009). The zebrafish embryo: a powerful model system for investigating matrix remodeling. *Zebrafish* **6**, 347-354.

Yang, E. V., Gardiner, D. M., Carlson, M. R. J., Nugas, C. A. and Bryant, S. V. (1999). Expression of Mmp-9 and related matrix metalloproteinase genes during axolotl limb regeneration. *Dev. Dyn.* **216**, 2-9.

Yates, C. C., Hebda, P. and Wells, A. (2012). Skin wound healing and scarring: fetal wounds and regenerative restitution. *Birth Defects Res. C Embryo Today* **96**, 325-333.

Yoo, S. K. and Huttenlocher, A. (2011). Spatiotemporal photolabeling of neutrophil trafficking during inflammation in live zebrafish. *J. Leukoc. Biol.* **89**, 661-667.

Yoo, S. K., Deng, Q., Cavnar, P. J., Wu, Y. I., Hahn, K. M. and Huttenlocher, A. (2010). Differential regulation of protrusion and polarity by PI(3)K during neutrophil motility in live zebrafish. *Dev. Cell* **18**, 226-236.

Yoo, S. K., Freisinger, C. M., LeBert, D. C. and Huttenlocher, A. (2012). Early redox, Src family kinase, and calcium signaling integrate wound responses and tissue regeneration in zebrafish. *J. Cell Biol.* **199**, 225-234.

Yoshinari, N., Ishida, T., Kudo, A. and Kawakami, A. (2009). Gene expression and functional analysis of zebrafish larval fin fold regeneration. *Dev. Biol.* **325**, 71-81.

Zakrzewska, A., Cui, C., Stockhammer, O. W., Benard, E. L., Spaink, H. P., Meijer, A. H. (2010). Macrophage-specific gene functions in Spi1-directed innate immunity. *Blood* **116**, e1-e11.

DEVELOPMENT